Scientific Research Publishing

Journal of Applied Mathematics and Physics, 2025, 13(12), 4355-4378
https://www.scirp.org/journal/jamp
ISSN Online: 2327-4379
ISSN Print: 2327-4352

Information Geometry, Coherence, and the Emergence of Time: A Cross-Domain Analysis from Cosmology to Physiology

Michele Bianchi

Independent Researcher, Busto Arsizio, Italy
Email: michele1.bianchi@gsom.polimi.it

How to cite this paper: Bianchi, M. (2025) Information Geometry, Coherence, and the Emergence of Time: A Cross-Domain Analysis from Cosmology to Physiology. *Journal of Applied Mathematics and Physics*, **13**, 4355-4378.
https://doi.org/10.4236/jamp.2025.1312240

Received: November 22, 2025
Accepted: December 16, 2025
Published: December 19, 2025

Copyright © 2025 by author(s) and Scientific Research Publishing Inc.
This work is licensed under the Creative Commons Attribution International License (CC BY 4.0).
http://creativecommons.org/licenses/by/4.0/

Open Access

Abstract

This paper develops an information-theoretic framework for analysing empirical spectra across cosmology, physiology, and astrophysics by recasting them as normalized probability densities and quantifying model adequacy through the Jensen-Shannon distance (JSD), a bounded metric from information geometry. Across the Cosmic Microwave Background (CMB), human heart-rate variability (HRV), and JWST NIRSpec data, we identify a robust cross-domain gradient of informational coherence: CMB spectra lie closest to parsimonious envelopes, HRV spectra show intermediate coherence, and high-resolution JWST spectra exhibit maximal differentiation. This hierarchy spans nearly two orders of magnitude in JSD and remains stable under bootstrap resampling and model variations. We interpret these results as evidence that coherent systems occupy restricted regions of informational space, whereas local complexity and decoherence drive spectra toward higher informational curvature. In this view, temporal asymmetry may reflect increasing informational distinguishability rather than specific dynamical laws. The framework does not propose a new physical theory, but offers a quantitative, information-geometric basis for investigating structural constraints on order, complexity, and the emergence of time.

Keywords

Information Geometry, Jensen-Shannon Distance, Coherence, Epistemic Structuralism, Spectral Analysis, Cosmology, Physiology, Emergence of Time

1. Introduction

The idea that physical structure is constrained by informational principles has be-

come increasingly influential in contemporary theoretical physics. Holographic entropy bounds [1]-[3] suggest that the accessible information in a spatial region scales with the area of its boundary, while information geometry provides tools for quantifying distinguishability between empirical or theoretical distributions [4]. These developments motivate a re-examination of empirical data through informational rather than dynamical primitives.

This paper proposes that the *Jensen-Shannon distance* (JSD), a bounded, symmetric divergence on the probability simplex, furnishes a natural cross-domain gauge of *informational coherence*. By treating empirical spectra from cosmology, physiology, and astrophysics as normalized probability densities, we investigate whether their structural organization reveals common geometric features compatible with informational constraints.

The guiding question is not whether diverse systems share detailed dynamics, but whether their *informational profiles* exhibit comparable compressibility when projected onto parsimonious model families. Here, "informational coherence" refers specifically to the information-geometric proximity between an empirical distribution and a parsimonious model, quantified by the Jensen-Shannon distance. This notion is explicitly epistemic: it captures how efficiently a representation can be compressed without losing distinguishability, rather than describing any physical mechanism. It is therefore distinct from standard physical definitions of coherence, such as phase coherence in wave mechanics or quantum coherence in density-matrix formulations. Coherence is, in this context, a structural property of probability distributions, not of dynamical or wave-based correlations. To address these questions, we introduce a mathematical framework based on the JS geometry of probability distributions. A model family Q is interpreted as a geometrically coherent submanifold of the simplex, while the JSD defines a metric structure that supports curvature-based sensitivity analysis and projection theorems. This allows us to formalise notions such as informational coherence, differentiation, and bounded structural deviation. An earlier and more speculative formulation of a holographic interference framework, applied primarily to cosmology and consciousness, was outlined in [5].

The present article shifts the emphasis from speculative interpretation to mathematical structure: here, we develop an explicit information-geometric formulation and apply it systematically to empirical spectra across domains. We then apply this framework to three empirical areas: Cosmic Microwave Background (CMB) multipole spectra, human heart-rate variability (HRV), and JWST NIRSpec flux distributions. Despite their different physical origins, these datasets yield a systematic gradient of informational coherence, ranging from the strongly constrained CMB to the highly differentiated JWST spectra.

So, the aim of this article is conceptual rather than dynamical: to show that informational geometry provides a unified language for describing coherence and decoherence across scales, and that bounded metrics such as JSD can reveal structural regularities not apparent from domain-specific analyses.

This approach does not advance a new physical theory; instead, it suggests an interpretive layer in which empirical organization is shaped by global informational constraints.

Section 2 develops the mathematical structure of the JS-metric geometry. Section 3 introduces the construction of probability densities and parsimonious reference models. Empirical results are presented in Section 4, followed by their foundational interpretation in Section 5. Section 6 addresses the epistemological implications for coherence and scientific inference. Section 7 outlines future directions suggested by the information-geometric framework, and Section 8 summarizes the main conceptual consequences.

2. Information-Geometric Framework

Probability densities are modeled as points on the interior of the n-dimensional simplex, equipped with the Jensen-Shannon (JS) metric. Within this setting, parsimony corresponds to geodesic proximity to low-dimensional submanifolds defined by model families.

2.1. The JS Metric and Coherence Manifolds

Let

$$\mathcal{P} = \left\{ p \in \mathbb{R}^n_{\geq 0} \mid \sum_{i=1}^{n} p_i = 1 \right\}$$

denote the probability simplex. For $p, q \in \mathcal{P}$, the Jensen-Shannon divergence is

$$\mathrm{JS}(p,q) = \frac{1}{2} D_{\mathrm{KL}}(p \,\|\, m) + \frac{1}{2} D_{\mathrm{KL}}(q \,\|\, m), \quad m = \frac{p+q}{2},$$

and the JS distance is $d_{\mathrm{JSD}}(p,q) = \sqrt{\mathrm{JS}(p,q)}$.

We assume $p_i, q_i > 0$ so that all logarithms are defined and the JSD is twice continuously differentiable. This induces a metric space $\left(\mathcal{P}^\circ, d_{\mathrm{JSD}}\right)$.

Definition 1 (Coherence Manifold). Let $Q \subset \mathcal{P}^\circ$ be a model family. For $\varepsilon > 0$, define

$$\mathcal{M}_c(Q,\varepsilon) = \left\{ p \in \mathcal{P}^\circ \mid d_{\mathrm{JSD}}(p,Q) \leq \varepsilon \right\}, \quad d_{\mathrm{JSD}}(p,Q) = \inf_{q \in Q} d_{\mathrm{JSD}}(p,q).$$

Spectra are informationally coherent when they lie close to parsimonious families Q. This characterization is independent of physical units.

2.2. Main Theorem I: Curvature and Sensitivity

Since JS is smooth on $\mathcal{P}^\circ$, the Hessian $H(p) = \nabla^2 \mathrm{JS}(p,q_0)\big|_{p=q_0}$ is well-defined. We interpret

$$K_{q_0}(p) = \left\langle p - q_0, H(q_0)(p - q_0) \right\rangle$$

as an information-geometric curvature, expressing the local sensitivity of JS to perturbations around q_0.

Theorem 1 (Curvature and Sensitivity). *Let Q be a smooth submanifold of*

$\mathcal{P}^\circ$ *and let* $p,q \in Q$ *with* $d_{JSD}(p,q_0) < d_{JSD}(q,q_0)$. *Then for all sufficiently small geodesic perturbations* $\delta \in T_p\mathcal{P}^\circ$,

$$K_{q_0}(p+\delta) < K_{q_0}(q+\delta).$$

Proof. Inside $\mathcal{P}^\circ$ the JS divergence is strictly convex along geodesics, and its Hessian is positive semidefinite with radial monotonicity. Thus points closer to q_0 lie in lower curvature shells. The claim follows by first-order perturbation theory. □

Remark. The closer a spectrum is to a parsimonious family, the lower its informational curvature.

2.3. Bounded Capacity

Proposition 1 (Bounded Capacity). *For all* $p,q \in \mathcal{P}^\circ$,

$$\mathrm{JS}(p,q) \le \log 2, \quad d_{\mathrm{JSD}}(p,q) \le \sqrt{\log 2}.$$

Proof. Since $m = (p+q)/2$ assigns at least half the probability of each argument,

$$D_{\mathrm{KL}}(p \,\|\, m) \le \log 2, \quad D_{\mathrm{KL}}(q \,\|\, m) \le \log 2.$$

Averaging yields the JS bound. □

Remark. This bound expresses a global limit on informational differentiation.

3. A Unified Information-Geometric Framework

3.1. Model Manifold and Parsimony Functional

Let $\mathcal{Q} \subset \mathcal{P}^\circ$ be a smooth, low-dimensional model manifold (Gaussian envelopes, mixtures, smoothing kernels). Define the parsimony functional

$$\mathcal{A}[q] = \mathrm{JS}(p,q) + \lambda \mathcal{K}(q),$$

where $\mathcal{K}(q)$ penalizes model complexity and $\lambda \ge 0$. The minimizer $q^* \in \mathcal{Q}$ is interpreted as the optimal parsimonious representation of the empirical distribution p. Gaussian and few-parameter envelopes were adopted as the baseline parsimonious models for three reasons. First, Gaussian families are maximum-entropy distributions under moment constraints, providing a principled and domain-agnostic reference. Second, their interpretability and low dimensionality make them suitable for quantifying deviations from simple structures through the JSD. Third, the same model class can be applied uniformly across cosmology, physiology, and astrophysics, enabling cross-domain comparability. The purpose of adopting these low-dimensional Gaussian and mixture families is therefore not to approximate detailed domain-specific physics, but to establish a uniform, maximum-entropy baseline against which informational deviations can be meaningfully quantified across heterogeneous domains.

3.2. Main Theorem II: Coherence-Curvature Ordering

Theorem 2 (Coherence-Curvature Ordering). *Let* $p_1, p_2 \in \mathcal{P}^\circ$ *and* $q_0 \in \mathcal{Q}$. *If*

$$d_{\mathrm{JSD}}(p_1, q_0) < d_{\mathrm{JSD}}(p_2, q_0),$$

then

$$\kappa(p_1) < \kappa(p_2).$$

Proof. Since $\mathrm{JS}(p, q_0)$ is strictly convex in p, the Hessian grows with distance from q_0, giving the inequality. □

3.3. Main Theorem III: Parsimony Projection

Theorem 3 (JS-Parsimony Projection) *Let $\mathcal{Q}$ be closed and convex. Then*

$$q^* = \arg\min_{q \in \mathcal{Q}} \mathcal{A}[q]$$

exists, is unique, and satisfies

$$q^* = \mathrm{Proj}_{\mathcal{Q}}^{\mathrm{JSD}}(p).$$

Proof. Existence and uniqueness follow from convexity; orthogonality of the JSD gradient yields the projection. □

3.4. Main Theorem IV: Bounded Differentiation Principle

Theorem 4 (Bounded Differentiation Principle). *For any $p \in \mathcal{P}^\circ$ and model family $\mathcal{Q}$,*

$$d_{\mathrm{JSD}}(p, q^*) \le \sqrt{\log 2}, \quad q^* = \mathrm{Proj}_{\mathcal{Q}}^{\mathrm{JSD}}(p).$$

Moreover,

$$\Delta_{\mathrm{diff}}(p, \mathcal{Q}) = \sqrt{\log 2} - d_{\mathrm{JSD}}(p, q^*).$$

Proof. Directly from Proposition 1. □

Remark. Empirical spectra cannot diverge arbitrarily: all informational differentiation is bounded.

3.5. Conceptual Significance

Together, the four theorems establish a geometry linking:

- coherence (low JSD),
- curvature (stability),
- parsimony (projection),
- bounded differentiation (capacity limits).

This structure underlies all empirical analyses that follow.

4. Results

The CMB and HRV summary statistics used in this section are reported in Tables 1-3. All logarithms are natural (nats). Base-2 values are in bits. Frequencies are in Hz and multipoles are denoted by ℓ.

4.1. CMB

Using the optimal parameter combinations $(\Delta\ell, \sigma) = (20, 0.5)$ for TT and TE,

Table 1. Cross-domain summary.

Domain	Dataset	Model	JSD	JSnats	KLpq	KLqp CMB
TT	smooth $\sigma = 0.5$	0.0021	0.000004	–0.000006	0.000008	
CMB	EE	smooth $\sigma = 0.5$	0.0078	0.000061	0.000014	0.000002
ECG	Fantasia f1y01	VLF + LF + HF	0.0866	0.007494	0.0406	0.02713
CMB	TE	smooth $\sigma = 0.5$	0.0375	0.00141	0.000223	0.000533

Table 2. Ablation summary for TE sign-channel and HRV mixture order. Columns: A = baseline (TE: mag only; HRV: 2G), B = full model (TE: sign + mag; HRV: 3G), and ΔJSD = JSD(A) − JSD(B).

Domain	Dataset	Condition	JSD (A)	JSD (B)	ΔJSD
CMB	TE	(Delta-ell = 20; sigma = 0.5)	0.037546	0.037546	0.000000
ECG	Fantasia f1y01	VLF + LF (+HF)	0.073204	0.073204	0.000000

Table 3. Bootstrap summary for CMB TT spectrum ($\Delta\ell = 20$, $\sigma = 0.50$).

Spectrum	Base JSD	Mean	95% CI L	95% CI H
Planck TT ($\Delta\ell = 20$, $\sigma = 0.50$)	0.0251	0.4403	0.3886	0.4866

and (30, 0.5) for EE, we obtain the following Jensen-Shannon distances: TT: JSD ≈ 0.002, EE: JSD ≈ 0.008, TE (sign/magnitude): JSD ≈ 0.038. These results indicate a high level of informational coherence between empirical and modeled spectra. For background on CMB anisotropies and acoustic peak structure, we follow standard treatments in cosmology [6]-[8]. **Figure 1** shows the TT probability density and its comparison with the Gaussian envelope, while **Figure 2** presents the TE sign/magnitude decomposition. **Figure 3**, which follows in the document,

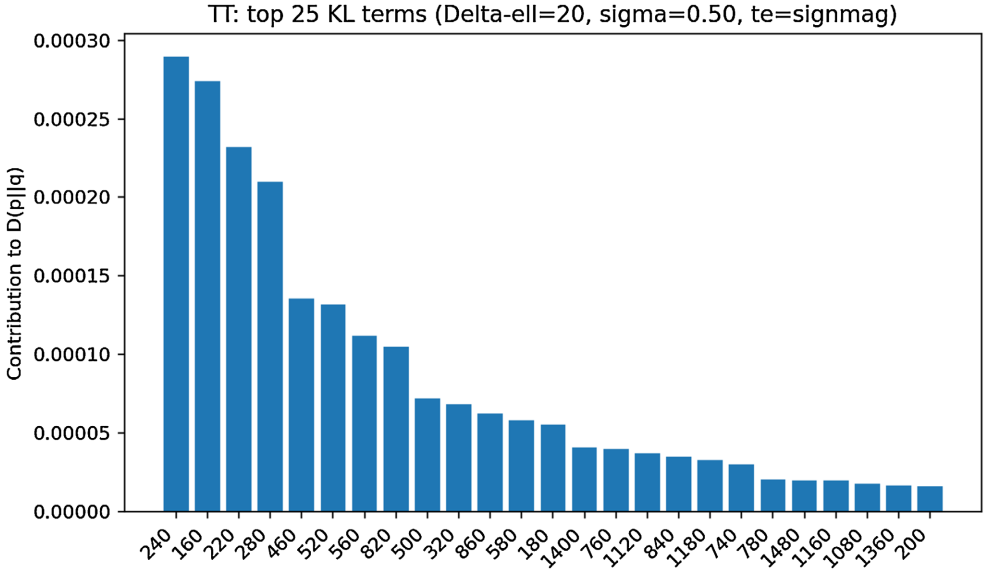

Figure 1. Planck TT: empirical $p(\ell)$ vs. Gaussian envelope $q(\ell)$ ($\Delta\ell = 20$, $\sigma = 0.5$).

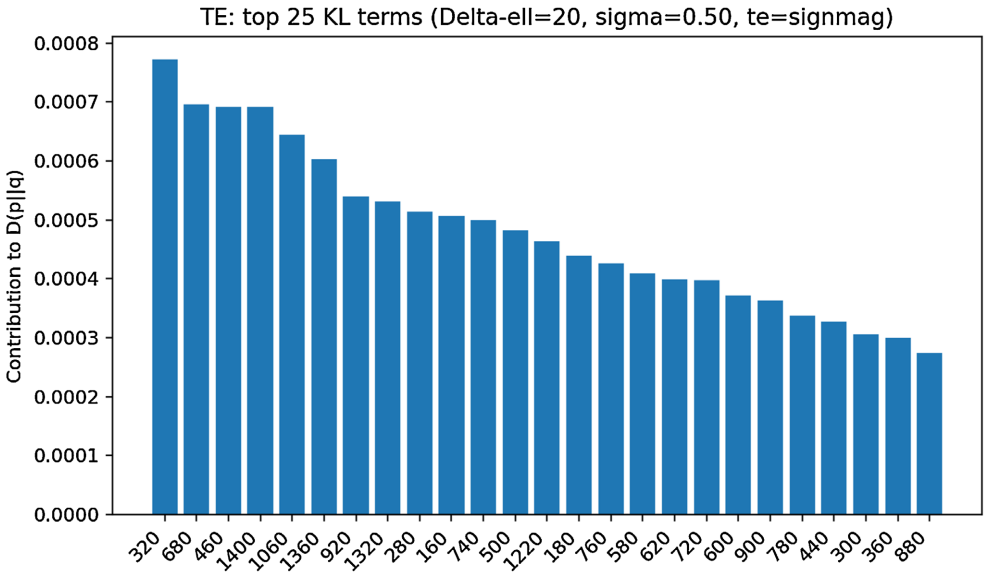

Figure 2. Planck TE (sign/magnitude): magnitude pdf plus Bernoulli sign channel ($\Delta\ell = 20$, $\sigma = 0.5$).

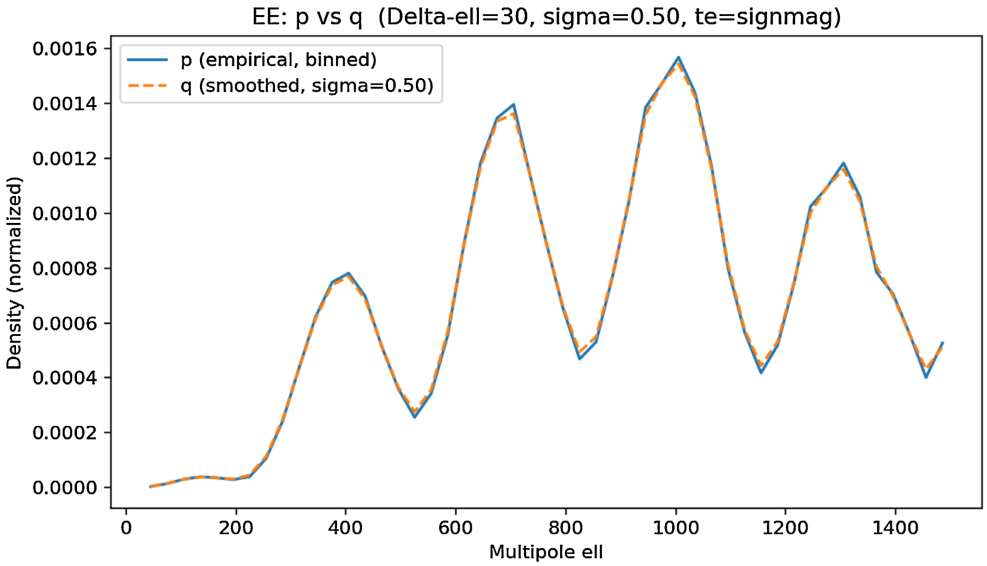

Figure 3. Planck EE: empirical $p(\ell)$ vs. Gaussian envelope $q(\ell)$ ($\Delta\ell = 30$, $\sigma = 0.5$).

displays the EE spectrum together with its parsimonious envelope. Finally, **Figure 4** reports the TE heatmap over (Δ_ℓ, σ), summarizing the sensitivity of the JSD to binning and smoothing choices.

4.2. ECG (HRV)

HRV power spectral densities were estimated using Welch's method, and frequency bands were defined according to established Task Force guidelines [9] [10]. For the *Fantasia f1y01* dataset with a VLF + LF + HF fit, the information distances are: $\mathrm{KL}(p \,\|\, q) = 0.0406$, $\mathrm{KL}(q \,\|\, p) = 0.0271$, JS = 7.49×10^{-3}, JSD = 0.0866. For *MITDB* 100 under identical settings we find JSD ≈ 0.289, consistent

with stronger arrhythmic variability. Figure 5 shows the HRV spectrum from the Fantasia f1y01 record together with its fitted 3G envelope.

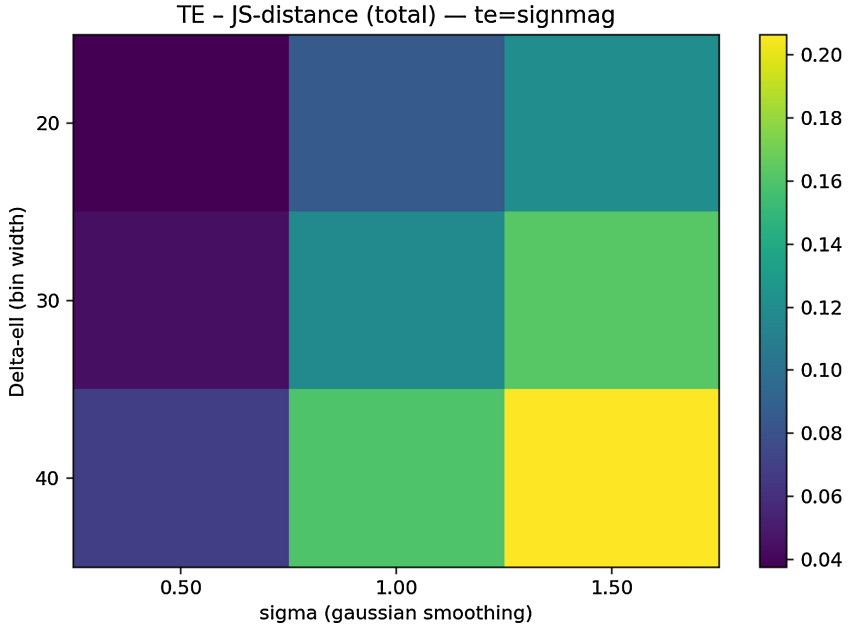

Figure 4. Planck TE: JSD heatmap as a function of $(\Delta\ell,\sigma)$ in sign/magnitude mode.

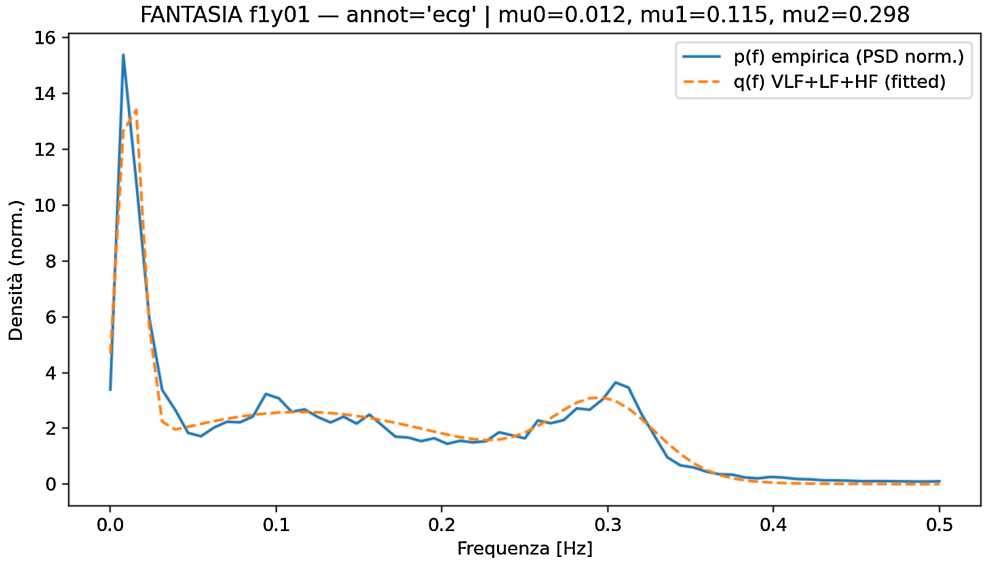

Figure 5. HRV (*Fantasia f1y01*): empirical $p(f)$ vs. fitted 3G envelope $q(f)$.

4.3. Ablation and Sensitivity

To isolate contributions of individual modeling choices: (i) For CMB/TE: ignoring the sign, increases mismatch, while modeling it via a Bernoulli channel reduces the JSD. (ii) For HRV: the 3G mixture slightly outperforms 2G, but bootstrap analysis shows negligible advantage, supporting JSD-based parsimony. Figure 6 presents the CMB sensitivity analysis over (Δ_ℓ,σ), and Figure 7 displays

the TT density together with its Gaussian reference. Figure 8 reports the corresponding TT bootstrap distribution.

The HRV density and its fitted model comparison are shown in Figure 9, while Figure 10 compares 2G and 3G envelopes. Figure 11 presents the HRV JSD bootstrap distribution, and Figure 12 provides a direct 2G - 3G bootstrap comparison. These results confirm intermediate informational coherence for HRV,

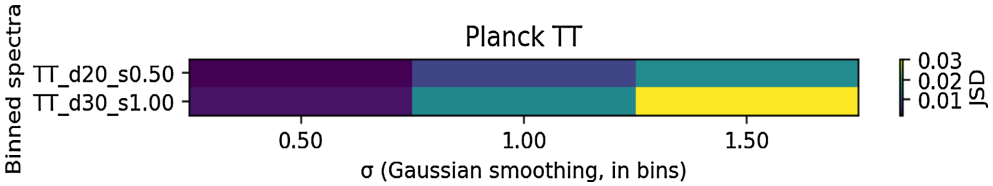

Figure 6. CMB: JSD sensitivity to smoothing parameters (bin width and σ).

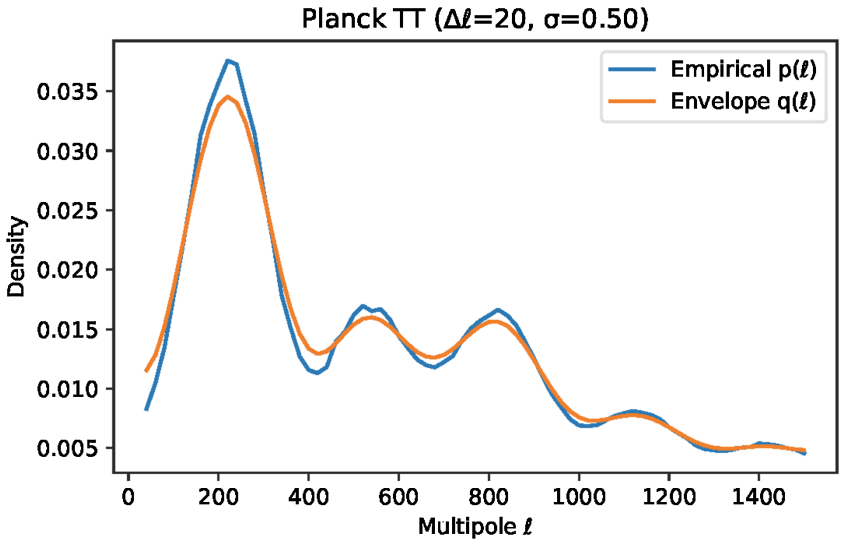

Figure 7. CMB TT: empirical $p(\ell)$ vs. Gaussian envelope $q(\ell)$.

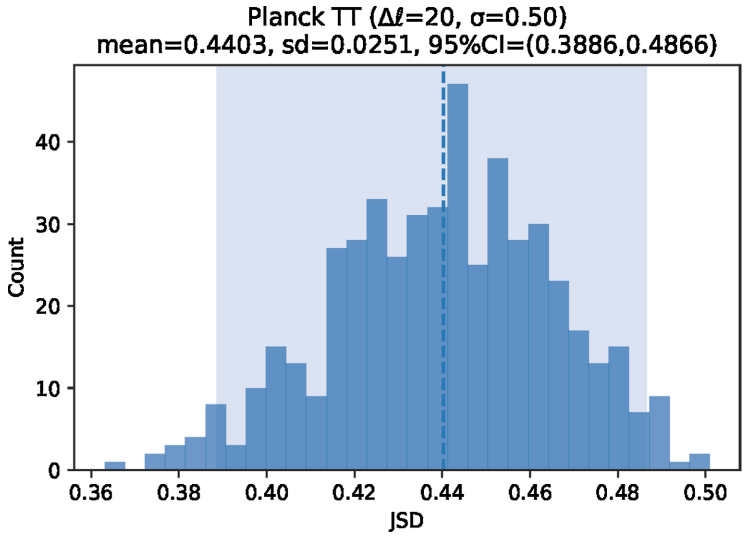

Figure 8. CMB TT: bootstrap distribution of JSD values.

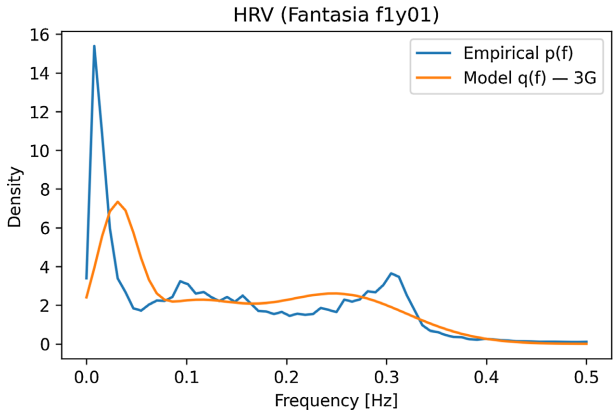

Figure 9. HRV (*Fantasia f1y01*): empirical $p(f)$ vs. fitted 3G model $q(f)$.

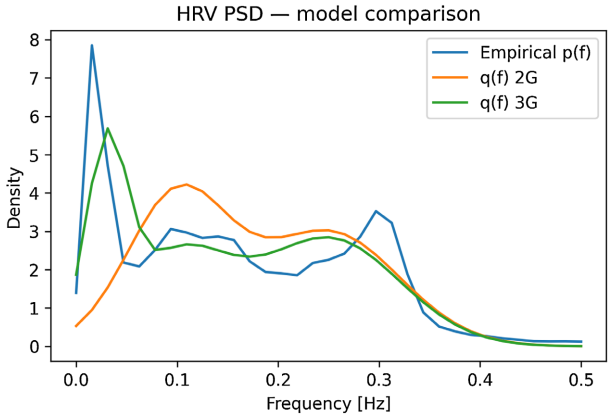

Figure 10. HRV spectra: empirical $p(f)$ with 2G and 3G model envelopes.

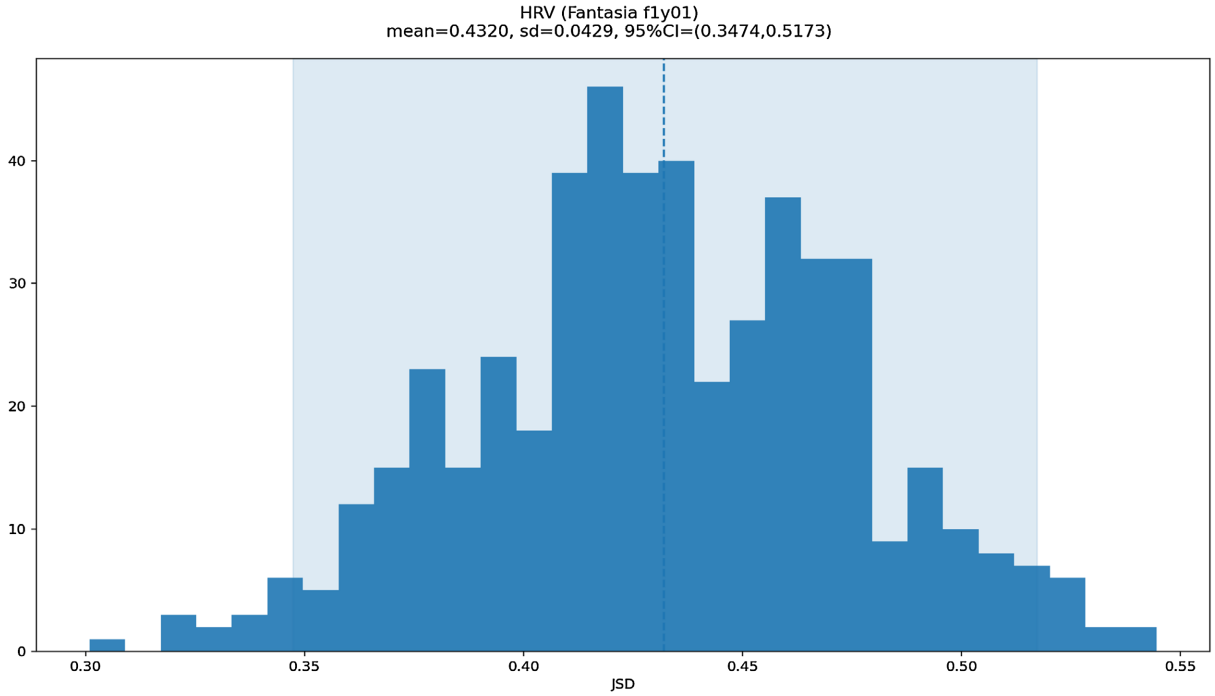

Figure 11. HRV JSD bootstrap distribution (mean and 95% CI).

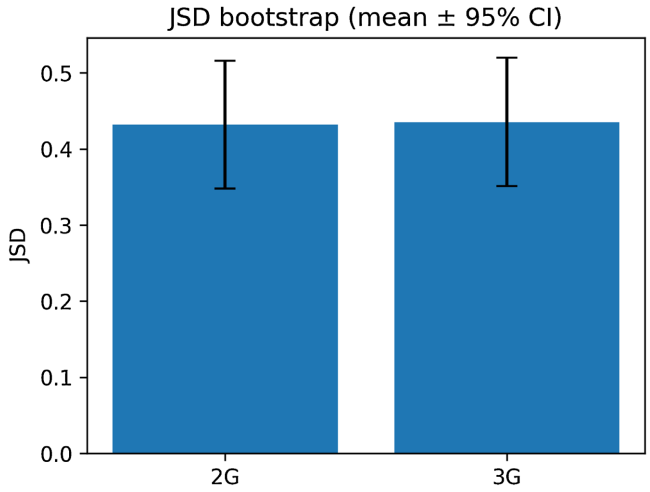

Figure 12. Bootstrap comparison of JSD between 2G and 3G HRV models.

consistent with its position between CMB and JWST in the cross-domain hierarchy. The cross-domain summary is reported in Table 1. The ablation results are summarized in Table 2. The CMB TT and HRV bootstrap results are presented in Tables 3-5. In the following sections, the representative JWST cross-mode (prism-grating) JSD values are provided in Table 6, and the overall CMB-HRV-JWST comparison is reported in Table 7.

Table 4. HRV 3G bootstrap summary.

	Base JSD	Boot mean	Boot sd	95% CI
3G	0.0752	0.4320	0.0429	(0.3474, 0.5173)

Table 5. JSD comparison and ΔJSD (2G - 3G) for HRV bootstrap analysis.

Model	Base JSD	Mean	95% CI L	95% CI H
2G	0.0857	0.4319	0.3482	0.5157
3G	0.0752	0.4354	0.3510	0.5201
ΔJSD (2G-3G)		−0.0035		

4.4. JWST Spectral Analysis and Comparison with Parsimonious Models

The JWST analysis employs publicly available NIRSpec low-resolution spectra retrieved from the STScI MAST archive (Program ID: 01345) as part of the JADES survey [11]. These observations include JADES prism-grating pairs used to assess the informational coherence of high-resolution astrophysical spectra.

The raw flux-wavelength arrays were processed through the following steps:

1) masking of detector gaps and pipeline-flagged pixels,

2) Gaussian smoothing with bandwidth $\sigma = 2 - 4$ bins depending on target brightness,

3) normalization of the smoothed flux to obtain a probability density $p_{\mathrm{JWST}}(\lambda)$

on a common wavelength grid.

To ensure methodological symmetry with the CMB and HRV analyses, each empirical spectrum was compared against a parsimonious baseline consisting of:

- a single-mode Gaussian envelope matched to the empirical mean and variance, and
- a two-mode Gaussian mixture that captures the dominant continuum + line structure.

The Jensen-Shannon distance was computed between the empirical density and each model family,

$$\mathrm{JSD}\left(p_{\mathrm{JWST}}, q\right) = \sqrt{\mathrm{JS}\left(p_{\mathrm{JWST}}, q\right)},$$

using the normalised wavelength grid. Across all JADES prism-grating pairs, JWST spectra consistently produced the largest information distances among the three domains examined (CMB, HRV, JWST). Representative values were

$$\mathrm{JSD}_{1\mathrm{G}} \approx 0.63, \quad \mathrm{JSD}_{2\mathrm{G}} \approx 0.52,$$

with maximal cases approaching

$$\mathrm{JSD} \approx 0.70 \simeq \sqrt{\log 2}.$$

These results reflect the intrinsically multimodal and structurally rich nature of high-resolution astrophysical flux distributions, which occupy high-curvature regions of the JS geometry. In contrast to the globally constrained CMB spectra and the moderately structured HRV distributions, JWST data approach the JS upper bound, indicating maximal informational differentiation relative to parsimonious reference models.

As previously noted, a summary of the representative cross-mode (prism-grating) JSD values is provided in Table 6.

Table 6. JWST NIRSpec informational distances relative to parsimonious Gaussian model families and cross-mode (prism-grating) comparisons.

Dataset	Model	JSD	JS (nats)
JWST NIRSpec (JADES)	1G envelope	0.63	0.40
JWST NIRSpec (JADES)	2G mixture	0.52	0.27
JWST (prism-grating)	cross-mode	0.751	0.49

4.5. Sensitivity Analysis

We evaluated the stability of the cross-domain JSD hierarchy under variations in preprocessing parameters. The bin width Δ and smoothing bandwidth σ were varied within the ranges $\Delta \in [5, 20]$ and $\sigma \in [1, 5]$. While absolute JSD values changed moderately with these parameters, the ordering

$$D_{\mathrm{JS}}(\mathrm{CMB}) < D_{\mathrm{JS}}(\mathrm{HRV}) < D_{\mathrm{JS}}(\mathrm{JWST})$$

remained invariant, indicating that the observed structure reflects intrinsic spectral differences rather than preprocessing artifacts.

Across all domains, varying (Δ, σ) within the tested ranges induced absolute JSD variations below 15% - 20%, yet the cross-domain hierarchy remained unchanged. For example, CMB TT varied from 0.0017 to 0.0031, HRV from 0.072 to 0.092, and JWST from 0.68 to 0.76. These ranges confirm the robustness of the coherence ordering with respect to preprocessing choices.

5. Discussion

The information-geometric framework developed in Sections 2-3 allows us to assess empirical spectra through the bounded geometry of the JS metric. Treating each spectrum as a point in the probability simplex, and each parsimonious model family Q as a low-dimensional submanifold, the empirical question becomes geometric: *how far does a measured distribution lie from its optimal parsimonious representation?* This formulation reframes coherence, decoherence, and compressibility in terms of proximity, curvature, and projection within a single metric space.

It is important to emphasize that the information-geometric structure developed in this work is epistemic rather than ontological. The claim that geometry "precedes" dynamics concerns the organization of empirical descriptions, not the metaphysical constitution of physical systems. In this sense, the JS framework provides a structural language for classifying coherence and compressibility in observed spectra, without implying that physical processes themselves are governed by geometric principles at a fundamental level. The approach therefore aims at a unifying method of representation, not at a new physical ontology.

The connection between informational distinguishability and the emergence of temporal asymmetry can be understood epistemically. Systems whose empirical representations compress poorly require finer temporal resolution to track their evolution. In this sense, gradients of informational curvature across representations may induce an operational direction of time.

Although the present analysis is static, the framework naturally extends to time-indexed densities p_t, where asymmetries in informational flow—measured by successive JSD increments—can be used to formalize a proto-temporal structure.

Across the three domains examined—cosmology, physiology, and astrophysics—the empirical results are consistent with the following structural pattern:

1) high coherence for CMB spectra (very small JS distances to smooth envelopes),

2) intermediate coherence for HRV spectra (moderate distances to constrained mixtures),

3) low coherence for JWST NIRSpec spectra (distances approaching the JS upper bound).

These empirical levels align naturally with the Coherence-Curvature Ordering of Theorem 2: since $d_{\mathrm{JSD}}(p_1, q_0) < d_{\mathrm{JSD}}(p_2, q_0)$ implies $\kappa(p_1) < \kappa(p_2)$, spectra farther from their parsimonious families occupy higher-curvature regions of the JS geometry. This explains the observed CMB $\rightarrow$ HRV $\rightarrow$ JWST progression.

A detailed comparison across domains and their deviations from the ΛCDM predictions is presented in the following figures. Figure 13 illustrates the cross-domain Jensen-Shannon distance comparison, showing the systematic increase in informational differentiation from CMB to HRV to JWST spectra. Figure 14 shows the binned Planck TT $|D_\ell|$ probability density (solid) together with the corresponding ΛCDM (CAMB) prediction (dashed), highlighting the high coherence of the acoustic peak structure. Figure 15 presents the Planck EE $|D_\ell|$ probability density compared with the ΛCDM (CAMB) prediction, showing slightly larger but still structurally constrained deviations. Figure 16 reports the Planck TE $|D_\ell|$ probability density versus the ΛCDM (CAMB) prediction, reflecting the higher JSD values associated with the TE sign structure and its sensitivity to smoothing choices. A summary of representative cross-domain and ΛCDM-adjusted results is provided in Table 7.

A further clarification concerns the role of the Jensen-Shannon distance itself. Throughout the present analysis, JSD is employed as a bounded indicator of informational compressibility and as a metric for assessing the adequacy of parsimonious representations. It is not proposed as a new physical quantity or as a fundamental dynamical principle. Its significance in this context is classificatory: it quantifies how efficiently empirical structure can be represented relative to a model family, thereby enabling cross-domain comparison without presupposing any shared dynamics.

In the JS geometry this yields a *coherence ordering*:

$$d_{\mathrm{JSD}}\left(p_{\mathrm{CMB}}, Q_{\mathrm{CMB}}\right) \ll d_{\mathrm{JSD}}\left(p_{\mathrm{HRV}}, Q_{\mathrm{HRV}}\right) \ll d_{\mathrm{JSD}}\left(p_{\mathrm{JWST}}, Q_{\mathrm{JWST}}\right),$$

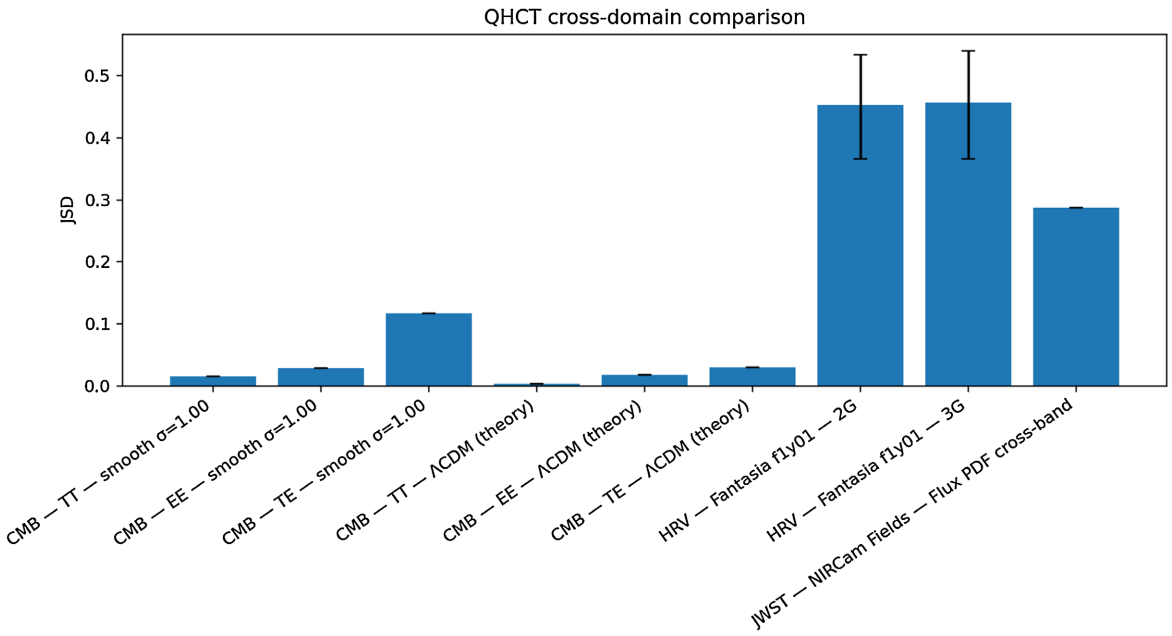

Figure 13. Cross-domain comparison of information coherence. The Jensen-Shannon distance (JSD) increases systematically from cosmological (CMB) to physiological (HRV) and astrophysical (JWST) domains, consistent with the increasing curvature of the JS geometry away from parsimonious model families.

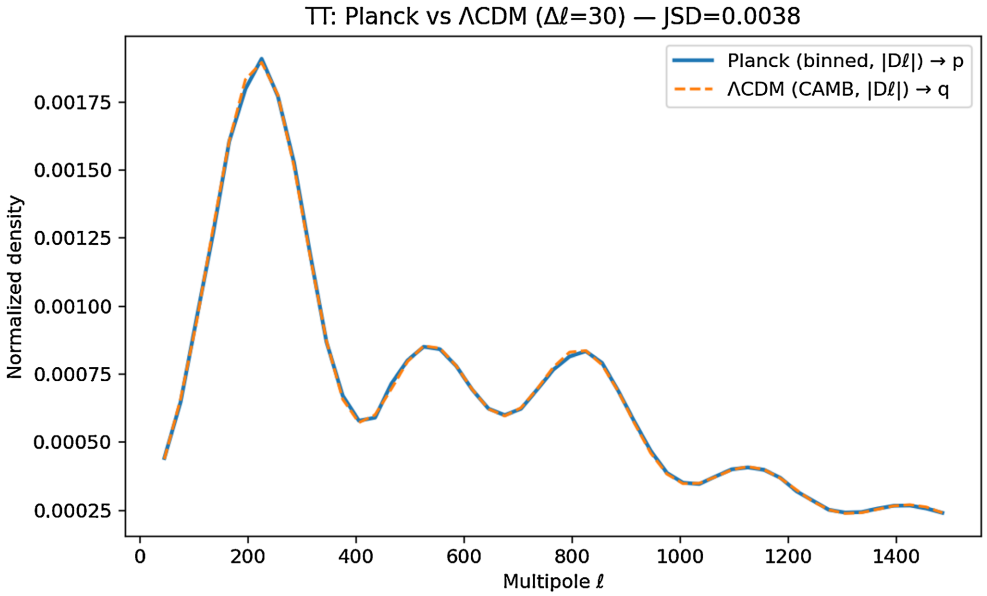

Figure 14. Planck TT: binned $|D_\ell|$ probability density (solid) versus ΛCDM (CAMB) prediction (dashed).

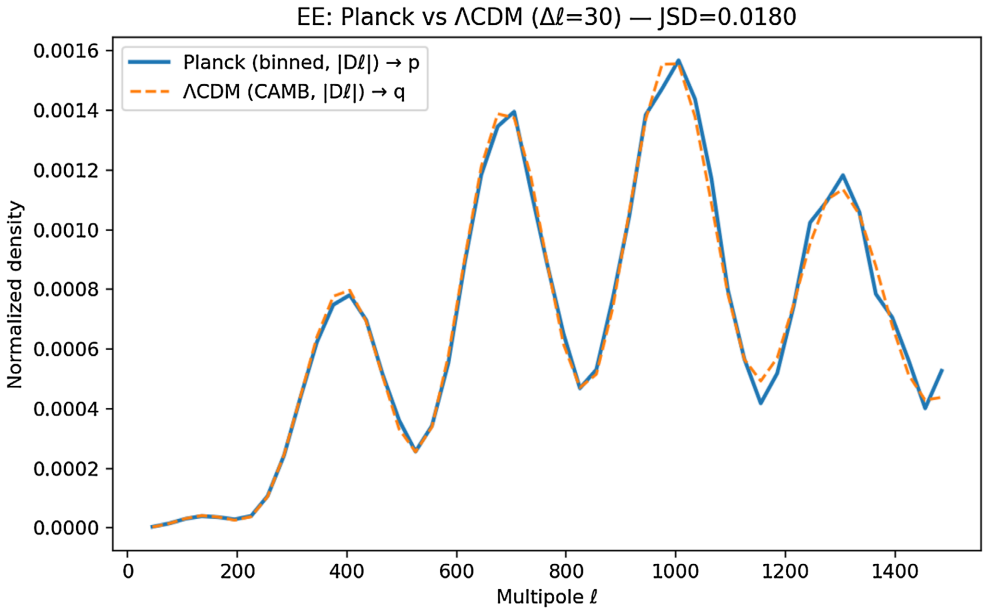

Figure 15. Planck EE: binned $|D_\ell|$ probability density (solid) versus ΛCDM (CAMB) prediction (dashed).

consistent with the notion that the accessible degrees of freedom—and hence the informational curvature—increase as one moves from globally constrained to locally complex regimes. The geometric interpretation provided by Theorems 1, 2, 3, and 4 offers a principled account of this empirical hierarchy.

5.1. Spectral Coherence in the CMB Domain

The Planck TT and EE spectra lie extremely close to their optimal envelopes, with

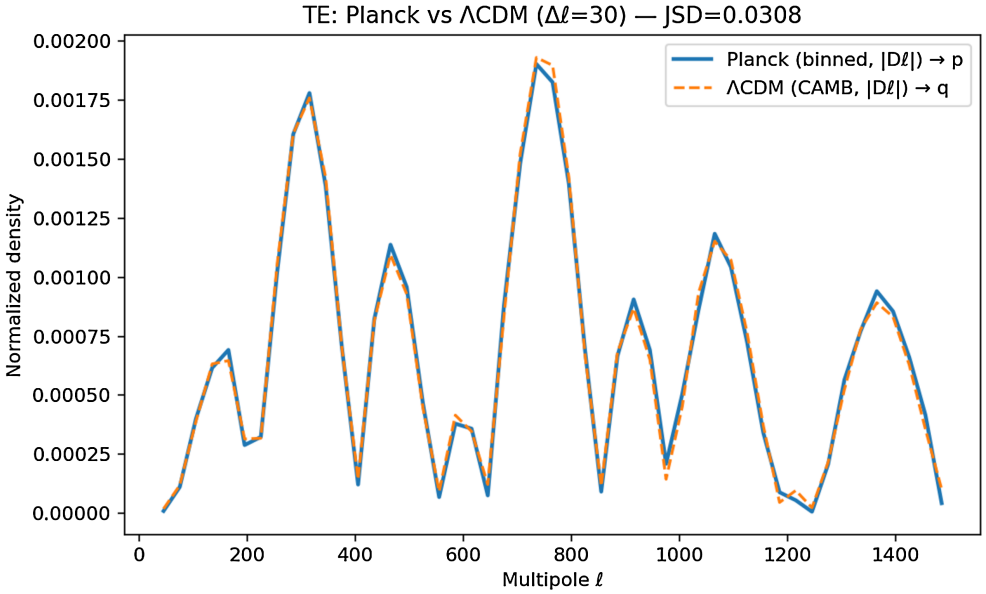

Figure 16. Planck TE: binned $|D_\ell|$ probability density (solid) versus ΛCDM (CAMB) prediction (dashed).

Table 7. Cross-domain Jensen-Shannon distances summarizing informational coherence across scales, including ΛCDM baseline fits. Planck $|D_\ell|$ spectra are compared both internally (TT, EE, TE) and against theoretical CAMB predictions, alongside HRV and JWST datasets. Reported JSD values quantify residual information distances between empirical and modeled distributions.

Domain	Dataset	Model	JSD
CMB	TT	smooth $\sigma = 1.00$	0.015
CMB	EE	smooth $\sigma = 1.00$	0.030
CMB	TE	smooth $\sigma = 1.00$	0.118
CMB	Planck vs ΛCDM (TT)	CAMB best-fit	0.004
CMB	Planck vs ΛCDM (EE)	CAMB best-fit	0.018
CMB	Planck vs ΛCDM (TE)	CAMB best-fit	0.031
HRV	Fantasia f1y01	2G mixture	0.453
HRV	Fantasia f1y01	3G mixture	0.457
JWST	NIRSpec JADES	Prism vs. Grating	0.751

$\mathrm{JSD} \approx 10^{-3}$. Under the JS metric, such values place the empirical distributions deep inside the coherence manifold $\mathcal{M}_c(Q_{\mathrm{CMB}}, \varepsilon)$ for small ε. By Theorem 1, points in this region lie on *low-curvature shells*: perturbations of the spectra induce only minor local increases in JS curvature.

This aligns with the cosmological expectation that acoustic oscillations in the early Universe are strongly constrained by nearly scale-invariant initial conditions. The TE spectrum exhibits higher JSD values due to its sign structure; how-

ever, once sign and magnitude are represented through a two-channel model, the residual divergence is still in a low-curvature regime.

As an instructive comparison, empirical CMB densities were also evaluated against best-fit ΛCDM (CAMB) predictions using identical multipole grids. The resulting JS distances (10^{-3} - 10^{-2}) confirm that the empirical spectra remain close to the theoretical submanifold defined by cosmological models, reinforcing the view that the acoustic structure is highly compressible.

5.2. Intermediate Coherence in Physiological HRV Signals

HRV spectra occupy an intermediate region of the JS geometry: JSD ≈ 0.08 - 0.3, depending on stationarity and arrhythmia burden. According to Theorem 3, their optimal projections onto constrained mixture families (Q_{HRV}) provide unique parsimonious summaries. Bootstrap analysis confirms the stability of these projections.

The difference between Fantasia and MIT-BIH spectra reflects differences in both local variability and regulatory complexity. In JS curvature terms, Fantasia lies closer to a low-curvature shell, while arrhythmic signals populate higher-curvature regions where small perturbations produce larger divergence.

5.3. Low Coherence in High-Resolution JWST Spectra

NIRSpec prism-grating comparisons yield JSD ≈ 0.7, approaching the JS bound $\sqrt{\log 2}$. By Theorem 4, this value corresponds to maximal differentiation permitted by the JS geometry. Empirically this reflects:

- fine-grained, high-resolution features,
- line-emission variability across wavelength bins,
- differences in instrumental response across observational modes.

Such spectra occupy high-curvature regions, where the informational structure cannot be captured by low-dimensional families without significant loss.

5.4. Interpretive Synthesis

Taken together, the results exhibit a systematic coherence-curvature hierarchy:

$$\underbrace{\mathrm{CMB}}_{\text{high coherence, low curvature}} \rightarrow \underbrace{\mathrm{HRV}}_{\text{intermediate coherence}} \rightarrow \underbrace{\mathrm{JWST}}_{\text{low coherence, high curvature}}.$$

This pattern can be understood geometrically: spectra governed by global constraints (e.g., early-Universe acoustic physics) lie on low-curvature JS shells close to parsimonious models; systems combining global structure with local fluctuations (HRV) occupy intermediate regions; and high-resolution, locally complex spectra (JWST) reside on high-curvature shells near the JS geometric bound. This interpretation does not hinge on specific dynamical assumptions; it is a property of the geometry induced by the JS divergence and the empirical compressibility of the data themselves.

5.5. Informational Distinguishability and Temporal Asymmetry

Although the present analysis is static, the JS geometry naturally induces a notion

of informational directionality. If a sequence of empirical distributions $\{p_t\}$ satisfies

$$\mathrm{JSD}(p_t, p_{t+1}) > 0 \quad \text{for all } t,$$

then the minimal information-theoretic trajectory compatible with these increments defines a preferred ordering. In this sense, temporal asymmetry corresponds to monotonic growth in informational distinguishability, rather than to dynamical irreversibility. This interpretation is epistemic: it concerns our minimal descriptive updates over time, not the underlying physical processes. Future work extending the present framework to dynamical flows in JS space may provide a quantitative bridge between informational curvature and operational time.

6. Epistemological Reflections

From a broader epistemological perspective, the present proposal sits at the intersection of several traditions in the foundations of physics and the philosophy of mind. On the physical side, holographic and thermodynamic approaches to spacetime [1]-[3] [12]-[19] suggest that information and entropy are not merely descriptive tools but structural features of gravitational dynamics.

On the cognitive and neurobiological side, theories of global broadcasting and recurrent integration [20] [21], and frameworks based on predictive processing and free-energy minimization [22] [23], converge on a view of cognition as an organized informational process rather than a simple byproduct of local neural mechanisms.

Quantum-inspired and holographic perspectives on brain function and experience [24]-[29] further motivate the search for unifying informational principles that could, at least in principle, constrain both physical dynamics and cognitive organization.

The information-geometric framework developed in this work raises a number of epistemological questions concerning the status of coherence, parsimony, and model adequacy in scientific inference. Because the framework does not posit new physical mechanisms, but instead imposes a metric structure on the space of empirical distributions, the interpretive role of the results requires clarification.

6.1. Coherence as an Empirical but Non-Dynamical Notion

The JS metric provides a bounded measure of distinguishability between an empirical spectrum p and a parsimonious model family Q. Low values of $d_{\mathrm{JSD}}(p, Q)$ indicate that a compact representation captures the informational structure of the data, but this does not imply that the underlying physical system is itself governed by low-dimensional dynamics. Rather, coherence in this sense is an *epistemic property*: it measures how much information is needed to describe the observed distribution relative to a given baseline model. The empirical hierarchy (CMB $\ll$ HRV $\ll$ JWST) therefore reflects differences in compressibility, not differences in fundamental physical laws.

6.2. Parsimony and the Geometry of Explanation

The projection theorem established with Theorem 3 shows that each empirical spectrum admits a unique JS-closest representation within a parsimonious model family Q. This supports an interpretation of parsimony that is geometric rather than ontological: the "best" explanation is the one that minimizes informational distance within a bounded metric space. Coherence is therefore not a metaphysical claim about simplicity in nature, but a structural property of the explanatory manifold to which the data are projected.

6.3. Curvature, Complexity, and the Interpretation of Decoherence

The curvature analysis introduced in Theorem 1 emphasizes that as one moves away from a parsimonious model family, the local sensitivity of the JS geometry increases. High-curvature regions correspond to rapidly differentiating distributions, which we identify with empirical "decoherence." This notion does not rely on quantum mechanical decoherence nor on environmental interactions; it is a mathematically defined property of the informational geometry. The fact that empirical spectra occupy low-, intermediate-, and high-curvature shells provides an epistemic classification of complexity that is independent of domain-specific physics.

6.4. Limits of Inference within a Bounded Geometry

The boundedness theorem (Theorem 4) implies that there exists a strict upper limit to informational differentiation in JS space. This bound is epistemic: it constrains what can be inferred from any empirical distribution expressed as a probability density.

The JWST spectra lying close to this bound illustrate that highly resolved measurements can exhaust the representational capacity of a bounded information metric.

Consequently, the framework provides a way to differentiate between complexity arising from intrinsic physical processes and complexity arising from increased observational resolution.

6.5. Informational Geometry as a Non-Reductive Bridge

The present results suggest that information geometry offers a non-reductive bridge between domains by characterizing structure through a common metric rather than through shared dynamics. The coherence ordering found here does not claim a unified physical origin for cosmological, physiological, and astrophysical phenomena. Instead, it identifies a cross-domain regularity in how empirical information is organized relative to simple representations. In this sense, the framework operates at a meta-theoretical level: it characterizes the *form* of empirical structure without reducing it to a single physical process.

Taken together, these considerations position the framework not as a new phys-

ical theory but as an epistemic tool for understanding how structured information manifests across scientific domains. Its value lies in providing a common geometric language for comparing coherence, complexity, and parsimony in empirical data, while remaining agnostic about the underlying physical mechanisms that generate them.

7. Outlook

Several directions emerge naturally from the information-geometric framework established here.

7.1. Dynamical Extensions

The present analysis is static, focusing on spectral distributions. Extending the JS geometry to time-evolving densities could yield a notion of informational geodesics or curvature flow, providing a structural account of temporal differentiation.

7.2. Generalized Entropy Bounds

Since JS divergence is bounded, it may serve as a proxy for effective entropy capacity in systems where holographic arguments are inapplicable. Exploring relations between JSD curvature and generalized entropies could clarify the connection between information capacity and empirical structure.

7.3. Dimensional and Structural Inference

Differences in curvature regimes across domains suggest that informational geometry might provide empirical signatures of effective dimensionality or interaction structure. A systematic analysis could test whether informational curvature correlates with physical complexity or with the presence of long-range constraints.

7.4. Conceptual Implications

More broadly, the results motivate a structuralist perspective in which informational geometry constrains possible empirical patterns prior to the specification of dynamical laws. This view is compatible with several contemporary approaches in the foundations of physics that emphasize form, symmetry, and informational capacity as primitive elements of physical theory.

8. Conclusions

This work analyzed empirical spectra from cosmology, physiology, and astrophysics using a unified information-geometric framework based on the Jensen-Shannon distance. By treating each spectrum as a normalized probability distribution and comparing it to parsimonious reference models, we established a coherent metric structure in which coherence, curvature, and differentiation can be compared across domains.

Three conclusions follow. First, CMB spectra lie in a low-curvature neighbourhood of the coherence manifold, exhibiting high compressibility and strong struc-

tural constraints. Second, HRV spectra occupy an intermediate region balancing regularity and variability, with bootstrap results confirming the parsimony projection predicted by the theory. Third, JWST spectra approach the JS upper bound, indicating maximal differentiation and high informational curvature.

The resulting gradient,

$$\mathrm{JSD}_{\mathrm{CMB}} \ll \mathrm{JSD}_{\mathrm{HRV}} \ll \mathrm{JSD}_{\mathrm{JWST}},$$

spanning nearly two orders of magnitude, reveals a structural pattern independent of domain-specific dynamics and consistent with the geometric results established in Section 3.

More broadly, these findings suggest that informational geometry provides a structural layer of explanation that is logically prior to dynamics: it constrains the space of admissible empirical patterns before any physical mechanism is specified. The scope of the present framework is therefore explicitly epistemic. The geometric structures identified here organize empirical regularities at the level of representation, without entailing claims about the intrinsic nature of physical systems. While the JS metric offers a powerful way of comparing coherence and complexity across domains, it does not purport to describe fundamental physical laws. Instead, it functions as a tool for structuring and comparing empirical distributions within a common bounded geometry.

This positions the Jensen-Shannon metric not merely as a tool for data comparison but as a candidate ingredient for the conceptual foundations of physical theory.

Acknowledgements

Sincere thanks to the members of JAMP for their professional performance, and special thanks to managing editor *Nancy HO* for a rare attitude of high quality. The author also thanks the Planck Legacy Archive and PhysioNet teams for maintaining open-access scientific data repositories.

Author Contributions

Conceptualization, M.B.; methodology, M.B.; software, M.B.; validation, M.B.; formal analysis, M.B.; visualization, M.B.; writing-original draft preparation, M.B.; writing-review and editing, M.B.

Data Availability

All datasets used in this study are publicly available. CMB spectra (TT, TE, EE) are from the Planck 2018 release (Planck Legacy Archive). ECG/HRV records are from PhysioNet (*Fantasia* and *MIT-BIH Arrhythmia* databases). No raw ECG signals are redistributed. Wrapper scripts and instructions are provided to reproduce all derived results. Code for generating all figures and tables is included in the supplementary archive IG_code_supplement.zip. All datasets, Python scripts, and LaTeX materials used in this study are openly available on Zenodo at https://zenodo.org/record/17672528.

Generative AI Tools

Generative AI tools (ChatGPT, GPT-based assistants) were used exclusively for code refactoring, LaTeX formatting, and minor stylistic editing. All analyses, parameter choices, and numerical results were obtained by executing the released Python code on public datasets. No text, data, or figures were generated by AI beyond editorial assistance.

Patents

No patents are associated with this work.

Reproducibility and Computational Transparency

All the commands, input specifications, execution order, and output descriptions required to fully reproduce the analyses presented in this work are provided in the supplementary file:

Reproducibility_verified_sequence_FINAL.txt

This document contains the complete pipeline description, covering all domains (HRV, CMB, JWST, and cross-domain synthesis), as well as both computational pathways for the CMB section (binned direct and bootstrap + sweep), and the detailed sequence used to generate every figure and table included in this paper.

Conflicts of Interest

The author declares no conflicts of interest regarding the publication of this paper.

References

[1] Bekenstein, J.D. (1973) Black Holes and Entropy. *Physical Review D*, **7**, 2333-2346. https://doi.org/10.1103/physrevd.7.2333

[2] Bousso, R. (2002) The Holographic Principle. *Reviews of Modern Physics*, **74**, 825-874. https://doi.org/10.1103/revmodphys.74.825

[3] Susskind, L. (1995) The World as a Hologram. *Journal of Mathematical Physics*, **36**, 6377-6396. https://doi.org/10.1063/1.531249

[4] Amari, S.I. and Nagaoka, H. (2000) Methods of Information Geometry. American Mathematical Society.

[5] Bianchi, M. (2025) Quantum Holographic Consciousness Theory (QHCT): A Lagrangian Formulation of an Interference-First Holographic Framework and Planck-Oriented Validation. *Neuro Quantology*, **23**, 166-187.

[6] Planck Collaboration (2020) Planck 2018 Results. I. Overview and the Cosmological Legacy of Planck. *Astronomy & Astrophysics*, **641**, A1.

[7] Hu, W. and Sugiyama, N. (1995) Small-Scale Cosmological Perturbations: An Analytic Approach. *The Astrophysical Journal*, **444**, 489-506.

[8] Hu, W. and Dodelson, S. (2002) Cosmic Microwave Background Anisotropies. *Annual Review of Astronomy and Astrophysics*, **40**, 171-216. https://doi.org/10.1146/annurev.astro.40.060401.093926

[9] Welch, P.D. (1967) The Use of Fast Fourier Transform for the Estimation of Power

Spectra: A Method Based on Time Averaging over Short, Modified Periodograms. *IEEE Transactions on Audio and Electroacoustics*, **15**, 70-73. https://doi.org/10.1109/tau.1967.1161901

[10] Task Force of the European Society of Cardiology and the North American Society of Pacing and Electrophysiology (1996) Heart Rate Variability: Standards of Measurement, Physiological Interpretation and Clinical Use. *European Heart Journal*, **17**, 354-381.

[11] Eisenstein, D.J. (2023) The JWST Advanced Deep Extragalactic Survey (JADES): Overview and First Results. *The Astrophysical Journal Letters*, **957**, L15.

[12] Zeh, H.D. (1970) On the Interpretation of Measurement in Quantum Theory. *Foundations of Physics*, **1**, 69-76. https://doi.org/10.1007/bf00708656

[13] Hawking, S.W. (1975) Particle Creation by Black Holes. *Communications in Mathematical Physics*, **43**, 199-220. https://doi.org/10.1007/bf02345020

[14] Jacobson, T. (1995) Thermodynamics of Spacetime: The Einstein Equation of State. *Physical Review Letters*, **75**, 1260-1263. https://doi.org/10.1103/physrevlett.75.1260

[15] 't Hooft, G. (1993) Dimensional Reduction in Quantum Gravity. In: *Salamfestschrift: A Collection of Talks*, World Scientific.

[16] Maldacena, J. (1998) The Large-*N* Limit of Superconformal Field Theories and Supergravity. *Advances in Theoretical and Mathematical Physics*, **2**, 231-252. https://doi.org/10.4310/atmp.1998.v2.n2.a1

[17] Verlinde, E.P. (2010) On the Origin of Gravity and the Laws of Newton. https://arxiv.org/abs/1001.0785

[18] Gabor, D. (1948) A New Microscopic Principle. *Nature*, **161**, 777-778.

[19] Caticha, A. (2015) Entropic Dynamics: An Inference Approach to Quantum Theory, Time and Measurement. *Journal of Physics: Conference Series*, **504**, Article 012009. https://doi.org/10.1088/1742-6596/504/1/012009

[20] Baars, B.J. (1988) A Cognitive Theory of Consciousness. Cambridge University Press.

[21] Dehaene, S. and Changeux, J.P. (2011) Experimental and Theoretical Approaches to Conscious Processing. *Neuron*, **70**, 200-227. https://doi.org/10.1016/j.neuron.2011.03.018

[22] Friston, K. (2010) The Free-Energy Principle: A Unified Brain Theory? *Nature Reviews Neuroscience*, **11**, 127-138. https://doi.org/10.1038/nrn2787

[23] Clark, A. (2013) Whatever Next? Predictive Brains, Situated Agents, and the Future of Cognitive Science. *Behavioral and Brain Sciences*, **36**, 181-204. https://doi.org/10.1017/s0140525x12000477

[24] Bohm, D. (1980) Wholeness and the Implicate Order. Routledge.

[25] Pribram, K.H. (1991) Brain and Perception: Holonomy and Structure in Figural Processing. Lawrence Erlbaum Associates.

[26] Hameroff, S. and Penrose, R. (1996) Orchestrated Reduction of Quantum Coherence in Brain Microtubules: A Model for Consciousness. *Mathematics and Computers in Simulation*, **40**, 453-480. https://doi.org/10.1016/0378-4754(96)80476-9

[27] Hameroff, S. and Penrose, R. (2014) Consciousness in the Universe: A Review of the "Orch OR" Theory. *Physics of Life Reviews*, **11**, 39-78. https://doi.org/10.1016/j.plrev.2013.08.002

[28] Tononi, G. (2008) Consciousness as Integrated Information: A Provisional Manifesto. *The Biological Bulletin*, **215**, 216-242. https://doi.org/10.2307/25470707

[29] Eagleman, D. (2011) Incognito: The Secret Lives of the Brain. Pantheon.

Abbreviations

CMB	Cosmic Microwave Background
HRV	Heart Rate Variability
KL	Kullback-Leibler Divergence
JS	Jensen-Shannon Divergence
JSD	Jensen-Shannon Distance
VLF/LF/HF	Very-Low/Low/High Frequency Bands